Surface speciation in microwave-assisted CO oxidation over perovskites - The role of water and activation pretreatment

Daniel Röhrens^{1,*}, Ahed Abouserie¹, Gianluca Dalfollo¹, Jannis Kahlert¹, Bangfen Wang¹, Ariel Augusto Schönberger², Stefan Pischinger², Peirong Chen³, David N. Mueller^{4,*}, and Ulrich Simon¹

* corresponding author

1 Institute of Inorganic Chemistry, RWTH Aachen University, Landoltweg 1a, 52074 Aachen,
Germany

- 2 Chair of Thermodynamics of Mobile Energy Conversion Systems, RWTH Aachen University, Forckenbeckstraße 4, 52074 Aachen, Germany
- 3 Guangdong Provincial Key Laboratory of Atmospheric Environment and Pollution Control, National Engineering Laboratory for VOCs Pollution Control Technology and Equipment, School of Environment and Energy, South China University of Technology, Guangzhou 510006, China

4 Peter Grünberg Institut, Forschungszentrum Jülich GmbH, 52428 Jülich, Germany

Keywords: Microwave-assisted catalysis, microwave heating of solids, CO oxidation, exhaust aftertreatment, XPS, XAS

Abstract:

As a model for the energy efficient aftertreatment of exhaust gas components, we studied the microwave-assisted (MW) CO oxidation over a (La,Sr)CoO_{3-δ} (LSC) perovskite oxide catalyst under dry and humidified conditions. We found that the use of a MW-based process can offer multiple advantages over traditional thermocatalysis in this scenario, as the nature of the MWsolid interaction offers quick, adaptive and energy efficient heating as well as improved yield and lower light-off temperatures. As found by combined CO and water MW-desorption experiments, the presence of technically relevant amounts of water leads to a competition for surface active sites and thus slows the reaction rate without indications for a fundamental change in the mechanism. Remarkably, the performance loss related to the presence of water was less pronounced in the MW-assisted process. Additionally, while we recorded a temperature dependent degradation of the reaction rate in extended MW-catalysis experiments both in dry and humidified conditions, it quickly recovered after a short reactivation MW-treatment. Our study confirms that surface reaction can be driven by the use of MW-radiation in a similar magnitude that can be achieved by thermal activation at significantly higher temperatures. The nature of the effect of the MWtreatment on the structural and electronic surface properties of the LSC material was investigated by X-Ray absorption (XAS) and X-Ray photoelectron spectroscopy (XPS). We found evidence for a significant structural, chemical and electronic reorganization of the oxide surface, possibly consistent with the occurrence of overheated surfaces or "hotspots" during MW-exposure, which may explain the increased catalytic and heating properties of the LSC after the MW-pretreatment.

The good catalytic performance, quick response to MW-heating and long-term stability of the catalyst all indicate the promising potential of a MW-based process for the energy efficient exhaust aftertreatment using noble-metal-free oxide catalysts.

1 Introduction:

Recently, the synthesis, production and application of fuels from bio-based carbon feedstocks, CO₂, and H₂ as feedstock in advanced combustion processes has gained increased attention ^{1, 2}. Since a change in fuel composition is associated with this aspect, also the composition of the exhaust gas and its temperature will be subject to changes ³. Thus, the development of novel catalysts and processes for an adaptive exhaust gas aftertreatment for the removal of carbon monoxide (CO), hydrocarbon and oxygenated hydrocarbon compounds and nitric oxides is necessary to explore. The development in this field is also driven by the need to replace the currently predominating noble-metal catalysts because of availability, toxicity and cost. Promising candidates were reported from multiple sources, notably based on metal oxides in the fluorite or perovskite crystal structures 4-6. Perovskite oxides have long been considered to be suitable substitutes for noble metal catalysts in a wide range of oxidation processes and especially Srsubstituted lanthanum cobaltite (LSC) showed particularly good characteristics, like semi- and metallic-conducting properties which were found to be descriptors in thermo- and electrocatalytic processes ^{4, 7-11}. For LSC, performance descriptors towards the oxygen evolution reaction (OER) activity largely revolve around the electronic structure close to the Fermi level ^{12, 13}, demonstrating that any catalytic cycle including redox reactions at the surface will be influenced by the surface electronic structure. Furthermore, the perovskite oxides show a remarkable tolerance for simultaneously high substitution of both crystallographic cation sites and this way it was shown that the catalytic properties could be adjusted by a targeted synthesis ^{9, 10, 14}. Dry CO oxidation to

CO₂ using LSC catalysts has been conducted recently both in conventional thermocatalysis¹¹ and in microwave-assisted processes¹⁵ exhibiting performance characteristics expressed as T_{50%} values of 125 - 150 °C which are competitive to state-of-the-art Pd/CeZrO₂ catalysts that show similar values¹⁶⁻¹⁸.

Direct microwave (MW) heating of solid catalyst materials can be considered a promising and potentially environmentally friendly alternative to traditional thermocatalysis as it allows for quick, targeted and energy-efficient heating of the reactive surface 19-22. Previously, we reported the establishing of a monomode MW-assisted catalysis setup and its utilization for the study of the CO-oxidation reaction over a La_{0.8}Sr_{0.2}CoO₃ (LSC-82) perovskite catalyst ²³. The catalyst material itself is directly heated, given sufficient MW-susceptibility, while the surrounding atmosphere remains widely unaffected. This has implications for the adsorption/desorption kinetics and selectivity, and this situation is different from conductively heated systems ^{19, 24}. Additionally, locally overheated areas, so called hotspots, or activation phenomena on the surface are reported ²⁵, which can positively affect the catalytic performance. MW-assisted heterogeneous catalysis setups have been used for a broad range of reactions with good results in catalytic performance 15, ^{20, 26-30}. Several reports show that certain oxides undergo a change in physical and chemical properties upon MW-excitation above a certain threshold, that lead to increased surface reactivity and improved conversion of MW-energy to heat, which may explain the favorable performance of certain MW-assisted processes ^{15, 23, 31, 32}. However, these promising properties of MW-assisted heterogeneous catalysis have been mostly conducted under dry conditions in laboratory settings. For more technically relevant conditions we have to consider the influence of water vapor, since water is always present in the exhaust gas of hydrocarbon-based combustion processes. This is particularly true in the case of MW-assisted catalysis as the effects may be even more complex

due to possible direct heating of water in the feed-gas or activation of adsorbed water, all of which can affect the reaction kinetics and product profile ³³. Furthermore, long-term degradation of the catalyst material under humidified reaction conditions at elevated temperatures has to be investigated as well, especially considering the application of a non-traditional heat source in the form of microwaves, which directly stimulate polarization losses within the material ³⁴.

The presence of water vapor has been shown to directly affect catalytic oxidation reactions, both in terms of conversion efficiency and selectivity in non-MW-settings ³⁵⁻⁴⁰. Depending on the catalyst material, water was found to either increase catalytic performance for noble metals ⁴¹ or decrease in the case of oxide catalysts ⁴². Furthermore, even within the class of oxide materials, these effects can be remarkably complex, as for example Wang et al. found dramatically decreased CO oxidation rates over a Mn/Co-oxide catalyst in the presence of water, yet at the same time strongly increased oxidation rates for formaldehyde ⁴⁰. Mechanistically speaking, the decrease in catalytic CO conversion over oxide catalysts can be related to the competition for surface adsorption sites, as water can bind to metal ions or oxygen vacancies, partially blocking O₂ or CO from reaching the surface, which was shown for similar oxidation reactions on perovskite oxides

In this study we report our results from MW-assisted and conventionally heated catalytic oxidation of CO over a La_{0.8}Sr_{0.2}CoO₃ (LSC-82) perovskite catalyst in the presence of water in the feed gas. The influence of water vapor on the catalytic performance and MW-heating behavior are presented and compared against corresponding experimental data from dry atmosphere. Special emphasis is given to the spectroscopic investigation of the structural effects brought about by the MW-irradiation of the LSC surface. For this, we conducted X-Ray absorption spectroscopy (XAS) and X-Ray photoelectron spectroscopy (XPS) experiments and found evidence for a significant

rearrangement in the surface region, which may explain the high activity of LSC in MW-catalysis. Additionally, the contribution of material and microstructural factors is discussed and structural and compositional long-term stability of the catalyst is evaluated. These results constitute a first step towards technically relevant conditions in analyzing the MW-assisted conversion of exhaust gas components from novel fuel sources.

The MW-assisted heterogeneous catalysis experiments were carried out in a monomode MW-

2 Experimental:

Microwave catalysis

flow reactor setup described in detail in a previous publication ²³. The monomode configuration utilizes a standing wave profile with a discrete frequency (2450 MHz; $\lambda = 12.24$ cm) and ensures a relatively homogeneous field distribution in the area of the solid catalyst in the center of the cavity. 200 mg of the oxide material (granulated to a particle size between 200 - 355 µm) are situated on a layer of quartz wool inside a cylindrical quartz tube with an inner diameter of 4 mm. The solid is heated directly by MW-radiation while the gas stream enters the quartz-reactor through a stainless-steel pipe, which is heated to 165 °C to avoid water condensation in the line. As the length of this heated line is relatively short and covers only the distance from the water injection to the MW-reactor, the temperature increase at the catalyst due to the presence of the heated line was found to be in the range of 1-3 °C. The exhaust of the flow-reactor is connected to an FTIR gas analyzer (GA 2030, MKS Instruments Deutschland GmbH, München, Germany) for the in-operando quantification of IR-active molecular species, i.e. CO and CO₂. The temperature of the MW-assisted catalysis is recorded inside the catalyst bed by means of a fiberoptic MWcompatible contact thermal sensor (FOT) (TS-3, Weidmann Technologies Deutschland GmbH, Dresden, Germany). This method of thermal sensing is superior to optical pyrometry, as we laid out in detail previously 23 . Before each conversion experiment, we conducted a pre-treatment in 100 sccm N_2 (5.0 purity) at 190 °C for 10 minutes. During the CO conversion tests, we used a gas mixture of 84 sccm N_2 (5.0 purity), 10 sccm O_2 (5.0 purity) and 6 sccm CO (9% in N_2 , 5.0) leading to a CO concentration of approximately 5000 ppm in an oxygen excess of 10% (N_2 bal.). The gas transport for the catalytic setups was facilitated through the use of mass flow controllers (G-Series MKS Instruments Deutschland GmbH, München Germany).

The concentration readings for CO and CO₂ were recorded after 5-10 minutes at the designated temperature, as stationary thermal and flow conditions are reached comparatively quickly in the case of MW-assisted catalysis. The gas stream was humidified using a dosing pump (Model CP-DSM, Vici Valco International AG, Switzerland) to directly inject ultrapure water into the heated gas line. The liquid water is thus evaporated and transported by the carrier gas into the reactor. The resulting water concentration is measured by the FTIR gas analyzer and adjusted by controlling the microdosing pump rotation. The MW-setup is depicted schematically in Figure 1.

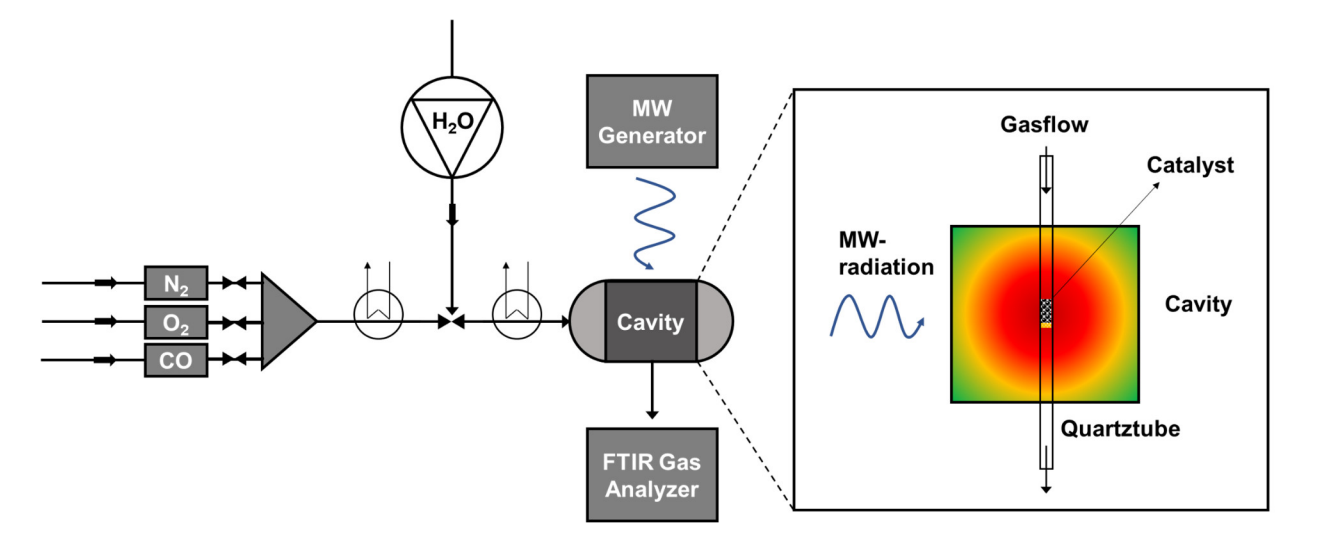


Figure 1. Schematic representation of the MW-catalysis and TPD experimental setup.

Thermocatalysis

The thermocatalytic CO conversion experiments were conducted in a temperature-controlled vertical oven (RS232, HTM Reetz GmbH), connected to the same FT-IR gas analyzer (GA 2030, MKS-Technologies Deutschland GmbH, München, Germany). To ensure comparability to the MW-experiments, we used again 200 mg of the LSC-82 catalyst granulated to 200 - 355 μm and placed it on a layer of quartz wool inside a quartz tube with an inner diameter of 4 mm. The temperature was recorded using a thermocouple inside the powder bed. Before each conversion experiment, we conducted a pre-treatment in 100 sccm N₂ at 220 °C for 1 hour (these conditions were selected because of the significantly longer time necessary for temperature equilibration in the conventionally heated furnace when compared to MW-heating). During the CO conversion tests, we used a gas mixture of 84 sccm N₂ (5.0 purity), 10 sccm O₂ (5.0 purity) and 6 sccm CO (9% in N₂, 5.0) leading to a CO concentration of approximately 5000 ppm in an oxygen excess of 10% (N₂ bal.). The gas transport for the catalytic setups was facilitated through the use of mass flow controllers (MKS Instruments Deutschland GmbH, München Germany) and we humidified the feed gas in the same way as was described for the MW-experiments above.

Catalytic performance:

The CO conversion was calculated based on equation 1:

CO conversion % =
$$\frac{C_{inlet,CO} - C_{outlet,CO}}{C_{inlet,CO}} \times 100 \%$$
 (1)

Where C_{inlet,CO} and C_{outlet,CO} are the CO concentrations corresponding to the inlet and outlet of the reactor, respectively.

The Arrhenius analysis was carried out by calculating first order rate constants for every catalytic experiment as a function of temperature and water concentration according to equation 2, which is valid for a plug flow reactor⁴⁴:

$$k = \frac{Q_0}{m} \times \ln(\frac{1}{1 - X_{CO}}) \qquad (2)$$

Where k denotes to the first order rate constant, Q_0 to the gas flowrate, m is the catalyst mass and X_{CO} : fraction of CO converted to CO_2 .

Temperature programmed desorption (TPD)

We conducted TPD experiments in the MW-setup described above using the LSC-82 catalyst. Three different desorption settings were probed: H₂O alone, CO alone and a mixture of CO and H₂O. The conditions described below are slightly different when compared to the catalysis conditions as we had to increase the mass of the oxide and decrease the flow-rate during desorption in order to obtain concentration peaks of significant magnitude.

We used 500 mg of granulated LSC-82 oxide which was placed inside a quartz tube onto a quartz wool bed. This tube was placed inside the microwave cavity in the same position as in the catalysis experiments, while the temperature was determined by optical pyrometry. Further, all three TPD-experiments were conducted in the following steps, which are depicted in Figure 2.

Pretreatment:

The sample was heated to 300 °C in dry oxygen (100 ml/min) for 1 hour. Subsequently, the oxide was allowed to cool down to room temperature in flowing nitrogen (100 ml/min).

Adsorption and saturation:

While the sample resided at room temperature (microwave off) in flowing nitrogen (100 ml/min) either 3.5 vol.% of water were fed into the gas stream by the usage of a water dosing pump into the heated gas-line in the case of the H₂O-TPD experiment and conversely by feeding dry 0.5 vol.% of CO in N₂ for the CO-TPD. For the combined H₂O-CO-TPD experiment the adsorption experiment was conducted by first applying the H₂O-TPD settings, directly followed by CO-TPD conditions. The adsorption phase continued until saturation was confirmed by monitoring the concentrations in the IR gas analyzer.

Purging:

After saturation, the feed gas was set to 100 ml/min dry nitrogen until both CO and H₂O were no longer detectable.

Desorption:

By controlled MW-heating (20 K/min) in 30 ml/min nitrogen the desorption behavior was recorded with the IR gas analyzer and analyzed as concentration vs. time -profiles for all three experiments.

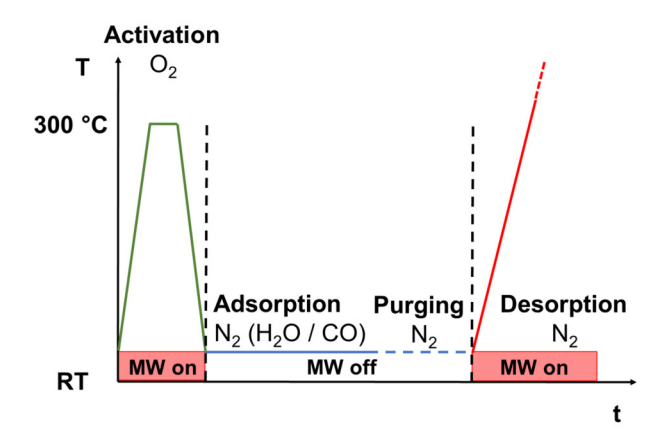


Figure 2. Schematic representation of the TPD experimental process conditions.

XRD

Powder X-ray diffraction (XRD) was performed using a STOE STADIP MP X-ray powder diffractometer (STOE and Cie GmbH, Darmstadt, Germany). The X-ray generator was equipped with a copper source operating at 40 kV and 40 mA, irradiating the sample with monochromatic CuK α (λ = 1.5406 Å). XRD patterns were recorded in transmission geometry at room temperature for 240 minutes over a 20 range of 10-90° with a step size of 0.015° employing an image plate position sensitive detector.

BET

The Brunauer-Emmett-Teller method (BET) was used to calculate the specific surface areas. The samples were degassed under vacuum (< 10⁻³ mbar) at 300 °C for 6 hours. Specific surface areas were determined by nitrogen adsorption at –196 °C using an automated gas adsorption analyzer (Autosorb iQ model 7 – Quantachrome Instrument, Anton Paar). BET surface areas were calculated using p/p0 points between 0.05 and 0.3 (small adjustments were made to obtain the best linear fit). Pore size distributions were obtained using the N₂ at 77 K on silica (cylindrical pore, NLDFT adsorption branch model) calculation model, in order to take into account the effects induced by cavitation and aggregation of plate-like particles. Data processing was performed using ASiQWin software (Version: 5.25).

XPS

Investigations of LSC-82 catalyst samples before and after humidified CO oxidation (both MW-and thermocatalysis experiments) using X-ray photoelectron (XPS) spectroscopy were conducted using an AXIS Supra instrument (Kratos Analytical Ltd.) with a hemispherical analyzer. During the measurements, the base pressure was $< 5.0 \times 10^{-6}$ Pa while a monochromatic Al K α radiation was used, and a simultaneous charge neutralization (low-energy, electron-only source) was applied to compensate for charging effects. The size of the probed sample area was $700 \times 300 \ \mu m^2$. Due to the magnetic nature of samples, the magnetic lens of the instrument was turned off and the lower intensity of detected photoelectron was counteracted by applying a high emission current of 25 mA for both survey and high-resolution (valence band (VB), Sr 3d, Co 2p and C 1s) scans. During the measurement of the survey scans a pass energy of 160 eV and a step size of 0.25 eV was used (5 sweeps, dwell time = 100 ms), while a pass energy of 20 eV and a step size of 0.05 eV was applied for the high-resolution scans (20 sweeps, dwell time = 200 ms). The BE scale of all samples for each individual element was calibrated with respect to the adventitious aliphatic C1s core level

at BE = 284.8 eV. The analysis of the spectra was performed in the CasaXPS software package (Casa Software Ltd.) by subtracting a Shirley background ⁴⁵ applying the sensitivity factors supplied by the instrument manufacturer for the quantification of the survey scans, and using a mixed Gaussian-Lorentzian (70%-30%) peak shape for the deconvolution of the Sr3d spectra..

XAS

Soft X-Ray Absorption spectra on as prepared and MW irradiated LSC were recorded on the UE56-1SGM beamline at the BESSY II electron storage ring in total electron yield mode at normal incidence. Background subtracted spectra were normalized to unity at the post edges at 555 eV (O-K-edge) and 800 eV (Co-L₃₂-edges), respectively.

SEM

Scanning electron microscopy (SEM) was performed on a FE-SEM LEO/Zeiss Supra 35 VP equipped with an Oxford Instruments INCA x-act detector. The samples were mounted on an aluminum stub with adhesive carbon tape.

3 Results & Discussion:

MW-induced activation

All MW-assisted catalysis experiments have been conducted after a short MW-based pretreatment that serves as an activation treatment of the catalyst material. As we have reported previously, both the heating behavior and the catalytic performance of LSC increased strongly upon reaching a threshold level under MW-excitation. At this point a drastic increase in temperature at constant MW-power was observed ²³. This observed phenomenon is very similar to reported findings in other published studies ^{15,31} and sometimes referred to as "thermal runaway" ^{46,47}. An example of a time series of this behavior is shown in Figure 3.

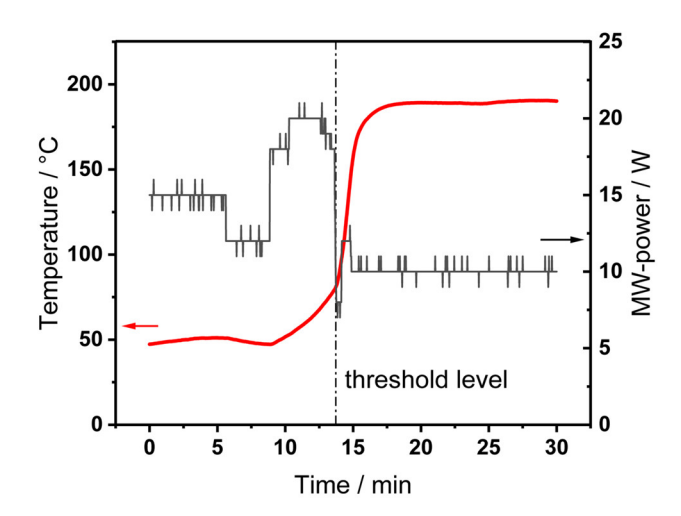


Figure 3. Time series of the MW-activation pretreatment of an LSC-82 sample in 100 sccm N₂. The temperature (red) has been recorded with a pre-calibrated pyrometer and is shown in conjunction with the manually set MW-output power.

As can be seen from Figure 3, the material undergoes a significant change with respect to its thermal response to the MW-electromagnetic field. Before the threshold level at around 85 °C the temperature rises slowly after manually increasing the MW-power. A decrease in power will naturally cause a decline in temperature (minute 5-8 in Figure 3). Shortly before the reaching of the threshold level, an increasing slope in the temperature curve is visible. Upon reaching the threshold level, the temperature rises very quickly at constant MW-power. To stabilize the temperature at the target value of around 190 °C the power had to be reduced drastically from 20 W to 10 W. The stable temperature of 190 °C at 10 W after reaching the activation threshold compares to around 50 °C at 15 W before the activation. This improved heating behavior encompasses both a faster thermal response towards changes in the MW-power as well as improved power efficiency, as evident by the higher temperatures per Watt. The activated state was retained for extended periods of time under dry conditions. In subsequent MW-assisted dry CO oxidation experiments with the MW-pretreated LSC-82 we found increased reaction rates and

consequently lower activation energy compared to the pristine catalyst as determined by an Arrhenius analysis (activation energy of 35.9 kJ/mol for as received LSC-82 and 23.1 kJ/mol for the MW-pretreated sample) ²³. All MW-assisted catalysis experiments in this study have been conducted with MW-pretreated (activated) samples.

MW-assisted and thermocatalytic CO oxidation, dry and humidified

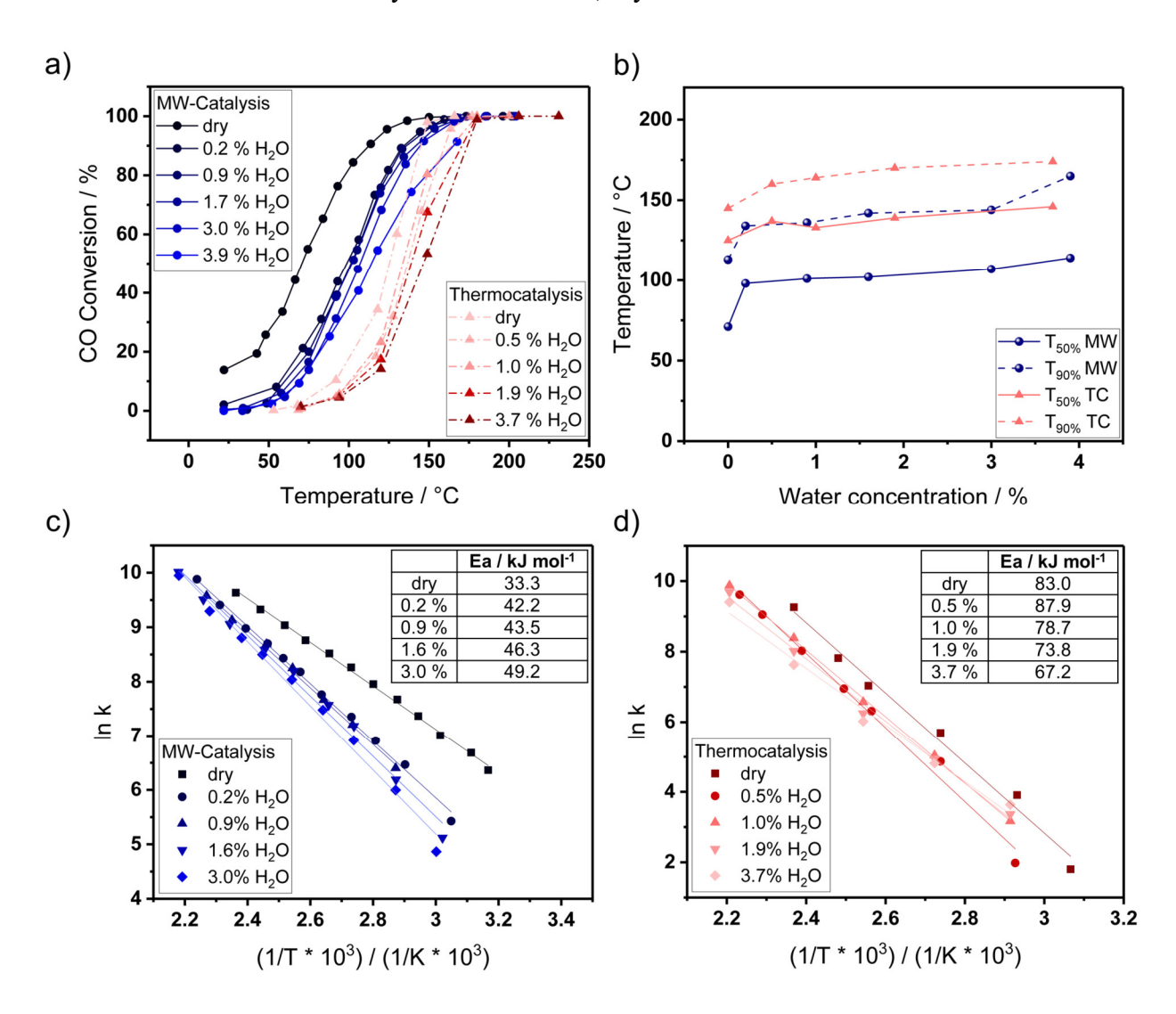


Figure 4. a) Performance curves for LSC-82 perovskite in MW-assisted- and thermocatalytic CO oxidation with varying water content. b) Corresponding characteristic T_{50%}- and T_{90%}-values. c)

Arrhenius analysis and derived activation energies for the MW-assisted CO oxidation and d) corresponding data for the thermocatalytic experiments.

The performance evaluation for the MW-assisted CO-oxidation reaction over an LSC-82 catalyst in dry and humidified atmospheres in comparison to thermocatalytic data is shown in Figure 4. The perovskite catalyst showed significantly higher performance in the MW-assisted process, with T_{50%} and T_{90%} values of 71°C and 113 °C, respectively compared to T_{50%} of 125 °C and T_{90%} of 145 °C for the TC-experiment (see Figure 4(b)). Additionally, after activation it was observed, that at room-temperature, notably without any MW-heating, a significant amount of CO conversion of 13.8% could be achieved, whereas no CO conversion was observed at roomtemperature for the thermocatalytic experiments. As can be seen from the Arrhenius plots (see Figure 4 (c) and (d)), the MW-assisted catalysis resulted in significantly lower activation energies determined by linear fitting of the logarithmic rate constants compared to the thermocatalytic experiments. Furthermore, the activation energy for the MW-experiments increased gradually with increasing water content in the feed gas, while the rate constant decreased with increasing water content for any given temperature. The same clear trend was not observed for the thermocatalytic experiments (see Figure 4 (d)), which first show an increase in activation energy at the introduction of water to the feed gas, but then followed by a decrease for the higher water concentrations. As the thermocatalytic Arrhenius analysis has less data points and a more pronounced scattering around the linear trend, the quantification of the activation energies in Figure 4 (d) should be interpreted with caution.

These findings could potentially be explained to result from a MW-induced reversible partial reduction of the oxide and thus from an increase in oxygen vacancy concentrations, as oxygen vacancies are a known descriptor in the CO oxidation over perovskite oxides ⁴⁸. As MW-induced

partial reduction of oxides has been reported before in the CeO₂-system ^{31, 32}, we believe a similar phenomenon to be responsible for the observed performance gain facilitated by the MW-based activation pretreatment in N₂ atmosphere we reported in an earlier publication²³, possibly via the route of strong local overheating (i.e. due to the formation of "hotspots"). A reduction of the oxide will result in more electrons in the catalyst and electronic charge carriers contribute to the MW heating behavior, effectively increasing the material's MW-absorption and conversion to heat. Thus, the additional electrons generated during the reduction could explain the increased heating behavior of the LSC after reaching a threshold temperature ("thermal runaway") presented before. A more detailed discussion is presented in the XPS and XAS surface analysis part of this study.

As soon as water is introduced to the gas supply, the catalytic performance decreases notably, both in MW- and TC-catalysis, which can be explained by a competition for active surface sites as was reported in similar reaction environments ^{35, 49}. While for the MW-catalysis a concentration of 0.2% already led to a deterioration of 27 °C and 21°C (T_{50%} and T_{90%}), we found that a further increase in water concentration up to 3.0% (MW) and 3.7% (TC) did only moderately affect the additional catalytic performance loss. This unexpected behavior could be the result of a promoting effect of surface hydroxyl groups formed in large enough quantities at this water concentration. The hydroxyl groups can affect the catalytic performance, which has been reported previously for CO-oxidation on single-atom-catalysts ⁵⁰, thus possibly roughly balancing out the negative effect of the reduction of the number of free surface sites.

Beyond 3.0% water concentration, the MW-catalytic performance suffered an increased loss, which may be related to macroscopic condensation of liquid water as we observed the water signal to become increasingly unstable thereafter. Because of technical limitations of our water dosing

setup and condensation phenomena at the unheated parts of the MW-reactor, we could not reach stable water concentrations higher than 3.9% or lower than 0.2%.

As can be seen from Figure 4, the effect of water on the catalytic performance curves is mostly symmetrical, i.e. low-temperature and high-temperature regions are affected nearly identically and the performance curves seem to be shifted to higher temperatures without a significant change in curve shape. Additionally, during all the catalytic measurements presented no side products (alcohols, aldehydes or carboxylic acids) were detected in our FTIR gas analysis indicating no fundamental change in the reaction mechanism for the humidified experiments. Only the MW-3.9 % measurement exhibits a change in the performance curve shape, which could indicate the beginning of water condensation related effects. This is also noteworthy, as increased water adsorption and retention on the surface was expected for temperatures below 100 °C and may be explained by the direct MW-interaction with water.

Figure 5 shows the steady-state MW-assisted dry CO oxidation at constant temperature near full conversion for several hours. The catalyst's activity was found to remain relatively stable under dry catalytic conditions with full CO conversion at 136 °C for a duration of 4 hours with only minimal performance degradation (0.5% per hour, see Figure 5). Interestingly, the activity could be fully recovered after a 5 minutes MW-treatment at 190 °C, which is the same value as in the MW-pretreatment step, which is shown in Figure 5. The treatment encompassed a very short increase in MW-power to reach a sample-temperature of 190 °C and subsequent return to the reaction temperature, after which full CO conversion was reached again. The following steady performance decline showed a comparable slope of about 0.5 %/h conversion loss to the first decline curve, indicating no changes to the surface reaction conditions. Thus, the observed degradation can be considered reversible and the elevated activity of the MW-pre-treated LSC-82

in MW-assisted CO oxidation can be quickly recovered by a corresponding increase in MW-power for a short duration.

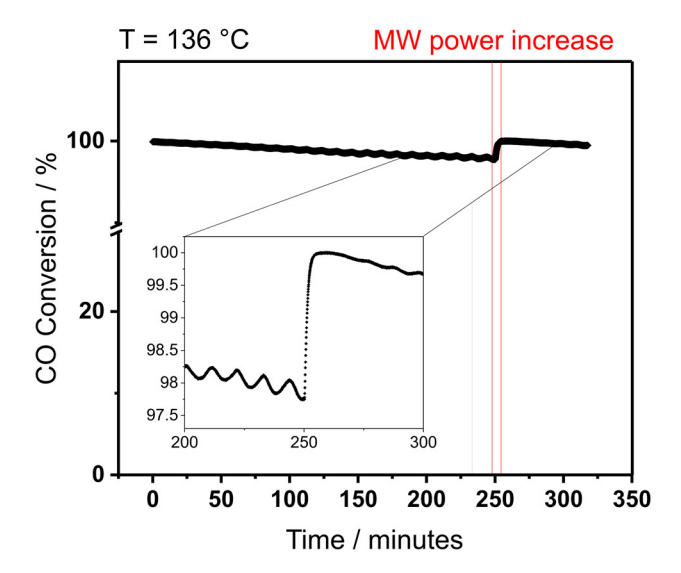


Figure 5. Steady-state MW-assisted dry CO oxidation at constant temperature near full conversion (136 °C) for 240 minutes and reactivation by a 5-minute MW-treatment by re-heating in the MW-setup to 190 °C followed by subsequent return to catalysis conditions at 136 °C. The performance oscillations in this graph result from temperature fluctuations of +- 5 °C as a result of the external cooler in the setup.

From these findings it can be concluded that MW-assisted catalytic oxidation proceeds at milder conditions and more efficiently after an activating MW-pretreatment when compared to corresponding thermocatalytic data. Water acts as a competitor for those surface-active sites, as is shown by MW-TPD experiments later in this study. The improved performance in the MW-experiments (compared to thermocatalysis) could be explained by a higher reservoir of available adsorption sites after the MW-pretreatment and/or other structural and electronic effects on the catalysts surface. This question is discussed in detail in the following surface spectroscopy chapter.

Spectroscopic surface analysis

We conducted XPS experiments on the as received pristine LSC-82 (AR), the same material after a MW-pretreatment as outlined in the previous chapter (MW) and an LSC-82 sample that had been subjected to MW-assisted CO oxidation conditions in humidified conditions for several days (MWH). The sample designation and respective MW-treatment is summarized in Table 1. The surface elemental composition and oxidation states of the catalysts were analyzed. Figure 6 (a) displays the XPS survey spectra for the three samples, indicating the presence of La (3d), Sr(3d), O (1s), and Co (2p). A Quantification of surface and bulk Sr from fitted XPS data is presented in Table S1, while Figure 6 (b) and Table S2 summarizes the surface atomic concentrations and ratios of the metal contents relative to oxygen, derived from the survey scans analysis. From the quantitative analysis a deviation from the ideal perovskite stoichiometric ratio is visible, indicating for example a relative enrichment of Sr-ions as compared to La and an apparent oxygen excess, as well as an A- to B-site cation ratio closer to 2:1 than the nominal 1:1. Additionally, Observations reveal an increase in the atomic percent (at.%) of all metal species (La, Sr, and Co) following exposure to MW irradiation, coinciding with a decrease in oxygen at.% when compared to the ARsample. Absolute percentage values need to be taken with caution, though, as the different core levels probe different depths due to variation in the kinetic energy of detected electrons and the near surface region most likely being inhmogenous, the trend of oxygen loss between samples however is clear. This would also explain the generally large oxygen excess as compared to the ideal perovskite composition (see Figure 6 and Table S2). In fact, thermally or electrochemically driven reduction of LSC have been found to to induce reversible Sr enrichment and possible precipitation of secondary phases such as (La,Sr)₂CoO_{4+δ}, ^{51,52} which would be more in line with the atomic abundances found here.

Table 1. Designation and treatment of the LSC-82 samples analyzed spectroscopically

Sample	Microwave treatment	Atmosphere
AR	none	n.a.
MW	10-minute MW-heating to 190 °C	dry N ₂
MWH	Multiple MW-CO oxidation experiments up to 200 °C	dry and humidified CO/O ₂ /CO ₂ /N ₂

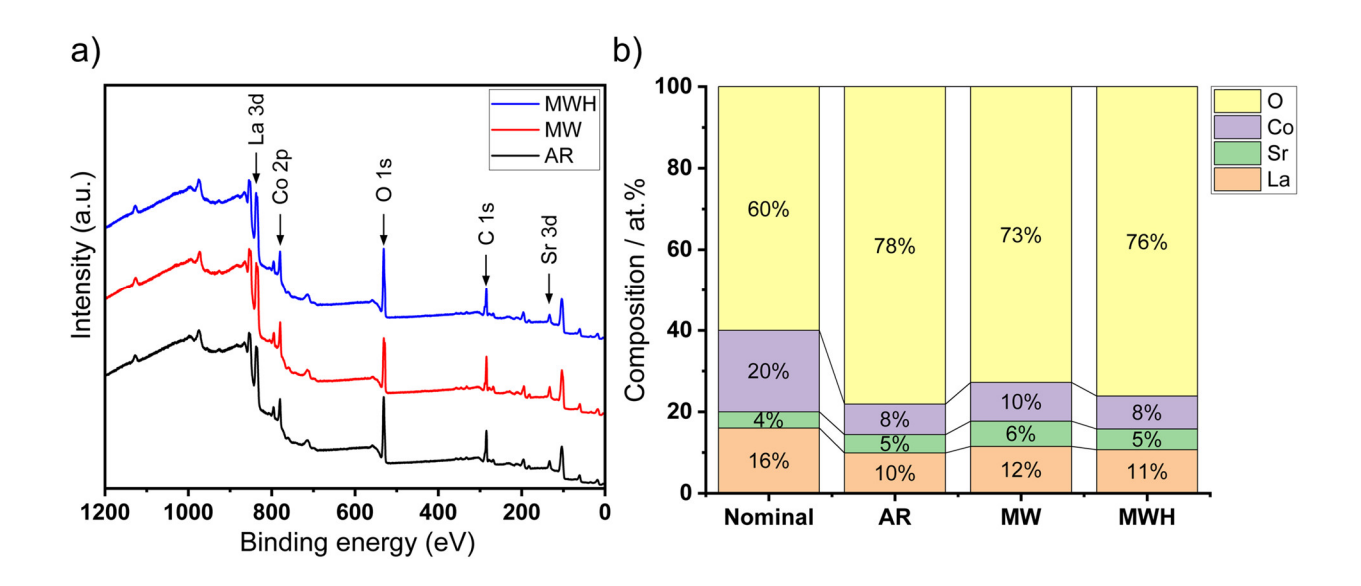


Figure 6. a) XPS-survey scan for the 3 different LSC-samples (AR: as received, MW: MW-treated, MWH: after MW-catalysis. b) Quantification of the elemental composition from these spectra.

Detailed spectra of the valence band (VB) and Co2p region for the three samples are shown superimposed in Figure 7 ((a) and (b), respectively). Here, we use difference plots (dashed lines) rather than pseudo quantitative fitting procedures to exemplify the evolution of the electronic structure with sample treatment, as due to being a strongly hybridized negative charge transfer material especially quantifying formal oxidation states of Co has little physical meaning ⁵³. Both spectral regions show similar evolution with sample treatment. Firstly, the VB region, which mostly consists of occupied O2p and Co3d states ^{12,54}, shows intensity variations at the top of the

valence band (BE 0-2 eV) between all three samples. This indicates changes in electron density close to the Fermi level, i.e. reduction and oxidation of the material ⁵³. Since the intercept of the VB maximum stays the same, no shifting of the Fermi level is occurring between samples. Focusing on the difference between the two MW samples (before and after H₂O exposure – purple dashed line) it can be seen that a singular, peak shaped component is changing, which can be attributed to the 3d⁶ ground state configuration, which is sharp ⁵⁵ as opposed to the charge transfer multiplet of the 3d⁷L configuration which would be spread over the whole range between 0-8 eV ⁵⁶. Simplified, this means that the change in electron density is localized to the Co. Concomitantly, the Co2p_{3/2} and Co2p_{1/2} signals at 780 and 795 eV, respectively, show intensity variation on the low BE flanks, which are not observed in reference hole doping experiments 55 and thus also indicate localized Co 3d state. The abundance of these states thus can be concluded to be a descriptor of the catalytic performance. Assigning a formal oxidation state or Co redox couple is ambiguous, as the 3d⁶ configuration points to Co³⁺, whereas a low BE component in the Co2p core levels is often attributed to Co²⁺ (3d⁷)⁵⁷, the latter comparison being disingenuous because those refer to binary oxides of completely different electronic structure than a (semi-)metallic perovskite such as LSC. Regardless of this and the exact process initiated by the MW irradiation, the catalytically active state just below the Fermi level, as deduced from comparing the MW and MWH samples and which is not (or only weakly) present in the AR sample is formed due to this process, giving a solid explanation of improved catalytic activity through MW activation.

Turning to the effect of the MW irradiation on the AR sample, we can make out the MW irradiation of the AR sample increases abundance of this electronic state significantly (red and blue dashed lines in Figure 7 (a) [valence band (VB)] and (b) [Co2p]), which leads to the conclusion that MW irradiation acts as a forming process for this catalytically active state.

Considering further additional changes between AR and MW, by we can find further contributions to the difference spectra (red and blue dashed lines) at \sim 7 eV in the VB and \sim 779 eV in the Co3p_{3/2} regions. Since especially the VB is convoluted in this region ⁵⁵, we used X-Ray absorption spectroscopy to gain further insights into the process.

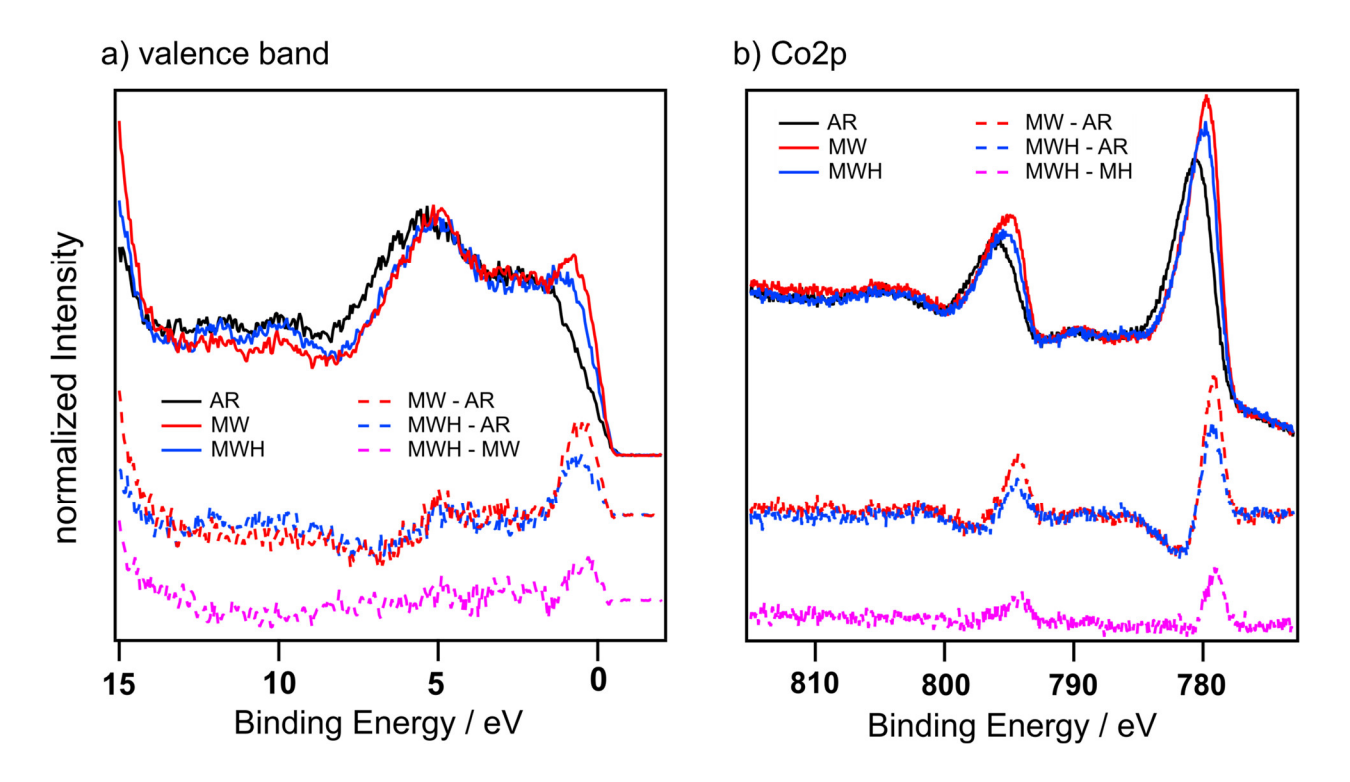


Figure 7. a) XP spectra and difference plots of the as received-(AR), MW-treated-(MW) and the MW-humidified catalysis sample (MWH) of the valence band. b) XPS spectra of the same samples in the Co2p region.

Figure 8 (a) shows the normalized oxygen K-edge spectra for both as received (black) and MW irradiated samples (red). The O2p-Co3d region (marked A, 525-530 eV) shows differences which are more complex than what has been found for simple oxidation or reduction of the CoO₆ manifold ^{58, 59} indicating departure from octahedral symmetry or changes in spin state ⁶⁰. The oxygen K-edge thus corroborates the findings from XPS that rather chemical surface

rearrangements than reduction or oxidation of the perovskite phase takes place. The Co-L₃₂-edges (Figure 8 (b)) in turn show an appreciable difference between samples with spectral weight shifting from the white line (marked D, 775 eV) to the pre-edge shoulder (773 eV). This is usually not observed in late 3d transition metal perovskites upon reduction or oxidation ⁵⁹, but has been reported in temperature induced spin state transition from $t_{2g}^{6}e_{g}^{0}$ (low spin, LS) to $t_{2g}^{4}e_{g}^{2}$ (high spin, HS) in LaCoO₃ ⁶¹, which is contradicted by the absence of changes in the O2p-Co4sp resonance in the O-K-edge (marked C, 538-548 eV). The XAS thus shows a complex interplay between changes in spin-state and/or local symmetry upon irradiation with MW, and it needs to be considered whether changes in near surface chemistry and structure are taking place. Here it should be noted that TEY XAS has a larger probing depth (around ten nm) than XPS (a few nm), so comparisons can only be qualitative. The photoemission spectroscopy shows a large A-site excess (~1.9 A- to B-site ratio) suggesting the presence of either A-site segregation and precipitation of e.g. SrO or Sr(OH) that is commonly observed upon thermal treatment of transition metal perovskites ⁶², or formation of a Ruddlesden Popper (RP) phase of A₂BO₄ stoichiometry, much closer to the surface stoichiometry observed in the XPS than ABO₃. The abundance of this RP surface phase has been shown to be reversibly dependent on temperature ⁵² and electrochemical oxidation and reduction ⁵¹, impacting electrocatalytic performance. It has to be noted however, that the previously cited studies observe the structural reorganization only after relatively harsh thermal treatment in the range of 500-800 °C, partly for extended periods of time, or strong electrochemical polarization, whereas our MW-exposed materials have not exceeded a temperature of 200 °C, at ambient pressure and without applying any electrochemical potential. The XPS analysis shows that both La/Sr and A/B ratios change upon MW irradiation, which is also corroborated by the O-K-XAS in the O2p-La5d/Sr4d region (marked B, 532 to 538 eV) 61 and

the intensity of the La-M₅₄ with respect to the Co-L₃₂-edges (Figure 8 (c)), indicating (because of the deeper probing depth of the XAS) that these rearrangements are not confined to the immediate surface. Additionally, the XPS analysis of the Sr3d region (see figure S1) exhibits significant changes between the AR, MW and MWH samples, which adds weight to the structural rearrangement results discussed before.

It is concluded, therefore that any presence and change in concentration of reduced Co species is related to this altered phase relation, in line with the general understanding that a formal Co²⁺ does not exist in a cobaltite perovskite ^{63, 64}. Since complex phase relations exist in the near surface region, we refrain from a quantification of oxygen vacancies, as this is only possible indirectly in well-defined systems ⁶⁵.

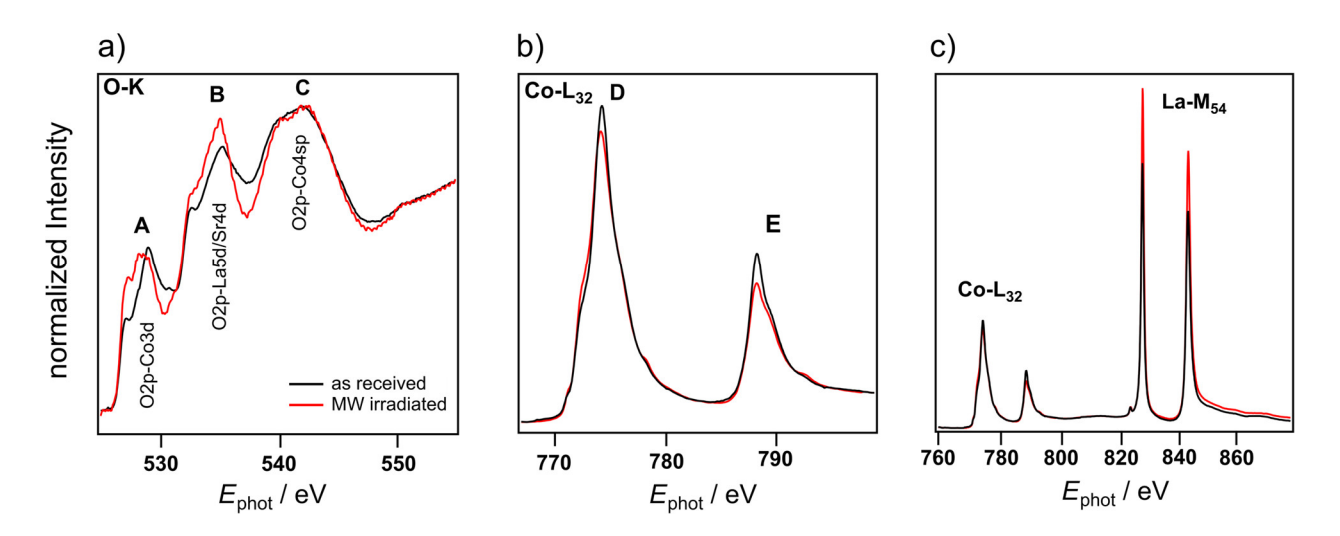


Figure 8. Soft-XAS data from LSC-82 as received (AR, black) and after MW-treatment (MW, red) in the O-K- (a), Co-L₃₂- (b) and La-M₅₄-region (c).

Mechanistic interpretation of the MW-pretreatment

The results from XAS analysis (in conjunction with the XPS) show changes in Co-spin state and surface chemistry after MW irradiation of the sample. Those changes are in line to those observed in similar perovskite samples after a pure thermal treatment at relatively high temperatures (450).

°C - 650 °C) ⁵¹. Additionally, the thermal creation of oxygen vacancies in bulk LSC in numbers sufficient to explain the increase in catalytic performance we observed, requires temperatures higher than 800 °C by a conventional heating in an atmosphere corresponding to our MWpretreatment ⁶⁶. These findings strikingly compare to the temperatures < 200 °C measured during the entire duration of MW-exposure (pretreatment and catalysis) by both contact and optical sensing methods. The previously mentioned hotspot-theory, i.e. a MW-induced strong local overheating of small or even sub-particle parts of the solid material ^{19, 25}, could theoretically explain both the observed structural changes and the improved catalytic performance. However, we did not find clear evidence for hotspots during the MW-experiments, as we recorded both stable volumetric temperature readings and long-term catalytic performance for up to several hours. As perovskites derived from LaCoO₃ are known to be reasonably good thermal conductors and the penetration depth of MW-radiation in this case is in the mm- to cm-range, thus covering the entire sample volume, the existence of significantly large areas of hot-spots with temperatures several 100 °C higher than the recorded volume temperature over extended periods of time, appears unlikely. Thus, this study potentially gives an indication for the existence of non-thermal contributions in driving surface reactions by MW-irradiation of solid catalysts.

MW-TPD experiments:

We conducted several TPD experiments under MW-excitation to investigate water adsorption/desorption behavior and its potential effect on the CO adsorption/desorption in a representative MW environment. Firstly, the pristine LSC catalyst was measured in H₂O-TPD (see Figure 9 (a)). From this experiment we could show a substantial water desorption peak, starting at around 60 °C and reaching a maximum at around 130 °C. The same catalyst material was subsequently used for a pure CO-TPD under MW-heating conditions. The CO desorption peak

was found to be sharp, with an onset temperature of around 80 °C and a maximum at around 100 °C (see Figure 9 (b)). Both CO and H₂O thus showed desorption in a very similar temperature range attained by MW-heating, but the H₂O desorption was slower as indicated by the width of the corresponding peak.

Interestingly, the CO desorption peak was significantly lower when we conducted a microwave CO-TPD experiment with an LSC sample which had been pre-saturated in humidified atmosphere (see Figure 9 (c)). While onset and maximum temperatures of the CO-peak remained close to the original dry CO-TPD, the total amount of CO desorbed was found to be much lower. This result indicates that water indeed competes for CO surface adsorption sites and thus the decrease in catalytic activity for humidified CO-oxidation experiments.

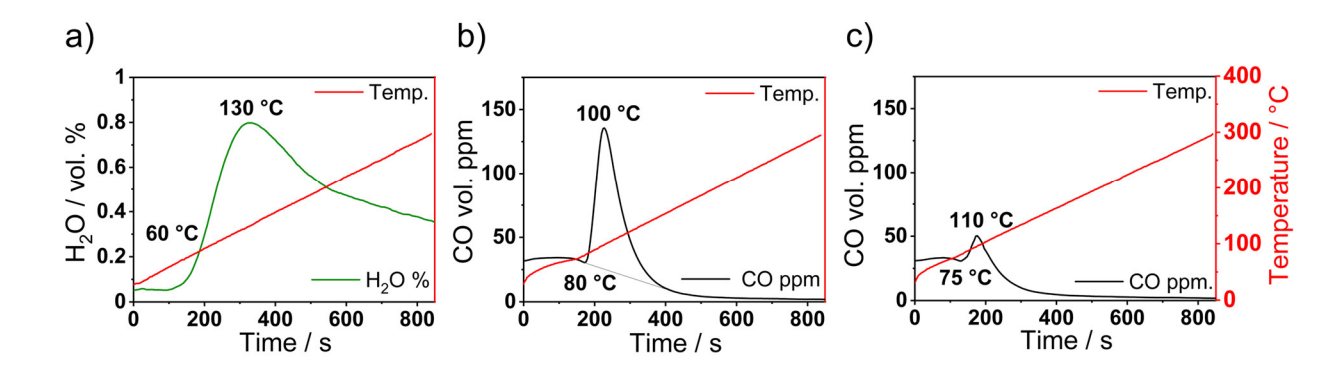


Figure 9. a) Water desorption profile from MW-TPD, b) CO desorption profile from MW-TPD and c) CO desorption profile from pre-saturated H₂O+CO-MW-TPD using the LSC catalyst material.

Structural/compositional analysis:

Analogous to the surface spectroscopy analyses, we conducted physisorption experiments on the as received LSC-82 material (AR), the LSC after a MW-pretreatment as discussed in the previous chapter (MW) and an LSC sample that had been subjected to MW-assisted CO oxidation

conditions in humidified conditions for several days (MWH). The results are summarized in Table 2. We found the total surface area as determined by the BET method increased slightly from the as received state (AR) of 14.4 to 18.5 m² g⁻¹ after the MW-based pretreatment in N₂ (MW). The LSC-sample after MW-catalysis experiments (MWH) again shows a decrease from the MW-pretreated state to a value of 14.3 m² g⁻¹ for the total surface area, which is nearly identical to the original state. No micropores had been detected in the three LSC samples. The detectable pore volume decreases from 0.093 cm³g⁻¹ for the AR LSC to 0.070 cm³g⁻¹ for the MW sample and furthermore to 0.052 cm³g⁻¹ for the MWH sample. This morphological change is consistent with the indications for a surface reorganization as found by our XPS and XAS analyses. A possible formation and growth of Sr-rich or Ruddlesden-Popper type secondary phases on the surface of the perovskite grains during MW treatment and subsequent morphological ageing under prolonged catalysis condidtions can explain these findings.

Table 2. Surface area analysis by physisorption following the BET method

Sample	Surface Area / m ² g ⁻¹	Pore volume / cm ³ g ⁻¹
AR	14.4	0.093
MW	18.5	0.070
MWH	14.3	0.052

To evaluate the long-term stability, both structural/compositional and in terms of catalytic performance, we examined the LSC-82 catalyst after an extended duration of testing (MWH), that involved all experiments shown above with MW-excitation. The material was thus exposed to dry and humid atmospheres with varying H₂O content and including CO for multiple hours per experiment, during a period of two weeks of testing. Additionally, the catalyst was rapidly heated

multiple times as part of the (re-)activation treatment. In spite of this environment and in contrast to the previous results (XPS, XAS, BET), the catalyst did not show any signs of structural change or irreversible degradation in terms of performance as can be seen in Figure 10, which reveals a near identical CO conversion performance in dry reference conditions before and after the extended humidified catalysis experiments. Additionally, the XRD patterns for both samples have been found to be single-phase, exhibiting exclusively reflections from the rhombohedral R-3c perovskite phase. Neither a binary oxide or hydroxide nor an indication for microstructural changes could be detected. This indicates that indeed the slight performance degradation as a function of time of 0.5%/h at constant temperature in MW-assisted CO oxidation is fully reversible and not associated with a compositional or structural change in the catalyst bulk. Changes to the surface however, are not detectable by XRD and it may be possible, that a slow structural degradation of the LSC-material may lead to secondary phase formation and performance degradation after much longer time exposed to reaction conditions.

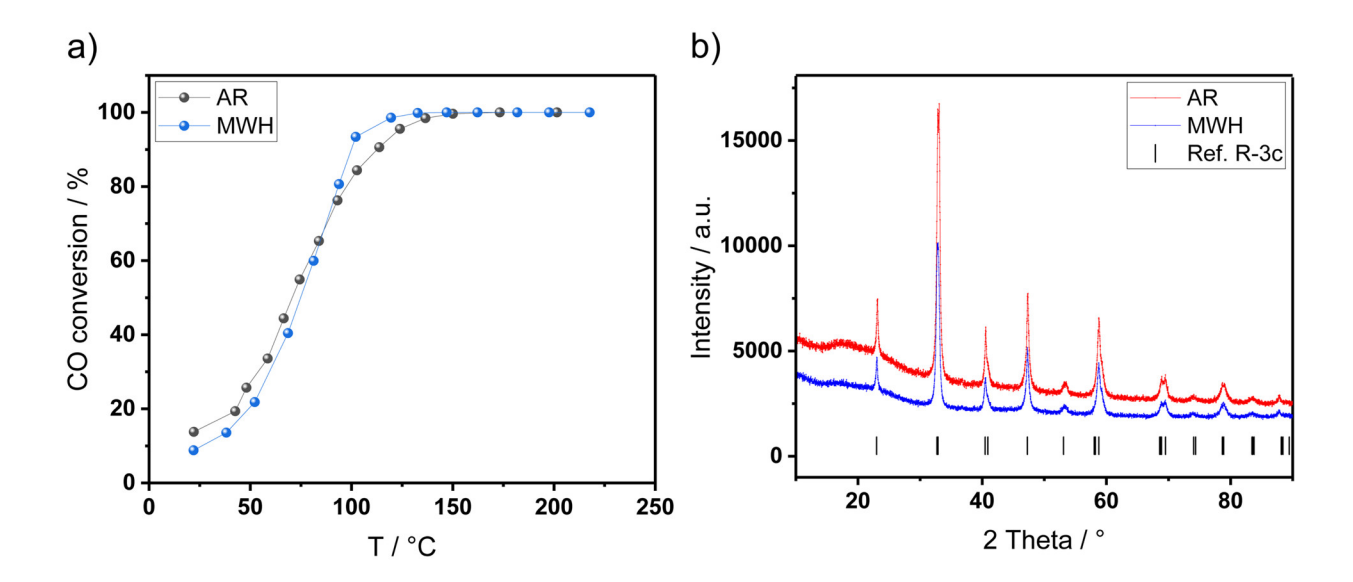


Figure 10. a) MW-assisted dry CO conversion of the as received LSC (AR) compared to an LSC catalyst after extensive testing in MW-heated humidified CO conversion conditions (MWH). b) XRD patterns for both samples and reference peak positions for the perovskite phase.

Additionally, we investigated the morphological state of the material by SEM. As can be seen in Figure S2, no apparent change is observable between the as received (AR) and the MW treated sample (MW). The sample after humidified MW-catalysis (MWH) looks very similar to the other samples with a slightly more granular surface.

4 Conclusions:

We have studied both the MW-assisted and thermocatalytic heterogeneous oxidation of CO over an LSC-82 perovskite catalyst in dry and humidified conditions in a lab scale test setup. In all experiments the lanthanum cobaltite showed a good catalytic performance, especially in the MW-assisted experiments, where we found light-off temperatures around 50 °C lower than in corresponding conventionally heated catalysis. This performance improvement was attained by a short MW-based pre-treatment in nitrogen atmosphere, which led to a significant surface reorganization as was shown by spectroscopic experiments. While the nature of the structural changes can be only discussed with limited certainty, from our results it is evident that the MW-based pretreatment leads to an electronic restructuring at the oxides surface, forming the catalyticly active electronic state, which would explain both the increased reactivity towards CO and the improved MW-heating properties.

Upon introduction of water into the catalysis, the performance dropped significantly, even for relatively modest amounts of water both in MW-assisted and conventional catalysis. The decrease showed a limited dependency with increasing water concentration over the tested concentration range. The MW-assisted catalysis was affected more strongly than the conventional catalysis, but

coming from a much higher base activity level the performance of the MW-assisted catalysis remained significantly better when compared to the thermocatalysis in the humidified experiments. Results from MW-assisted humidified CO-TPD give further support for the hypothesis of a competition for surface sites between CO and H₂O.

The LSC-catalyst showed a slow and fully reversible performance degradation under MW-assisted CO oxidation conditions (dry and humidified), which could be recovered by a relatively short increase in MW-power. This degradation coincides with a small decrease in surface area, compared to the MW-treated state, consistent with an ageing of the catalysts surface. However, we found no indication of either bulk-structural, -compositional or irreversible performance degradation of the LSC catalyst, both in MW-assisted and conventionally heated catalysis.

We thus conclude, the MW-assisted oxidation of CO over an LSC perovskite catalyst shows promising performance characteristics and may constitute an alternative to traditional thermocatalysis involving noble metals. The rapid, responsive and efficient nature of the MW-heating, combined with these findings, make MW-assisted catalysis using tailored metal oxides an abundant field of research for adaptive chemical conversion using alternative forms of energy input and the development of related processes on a technical scale.

ASSOCIATED CONTENT

Supporting Information. XPS Sr3d data and fitted contributions from surface and bulk Sr; Quantification of surface and bulk Sr from fitted XPS data; Quantitative evaluation of surface composition from the XPS-spectral analysis for as received and MW-treated samples; SEM images of the three investigated modifications of the LSC catalyst material (file type PDF).

ACKNOWLEDGEMENTS

This study was funded by the Deutsche Forschungsgemeinschaft (DFG, German Research Foundation) under Germany's Excellence Strategy – Cluster of Excellence 2186 "The Fuel Science Center" – ID: 390919832. The authors thank the team of the mechanical workshop of the Institute of Inorganic Chemistry at RWTH Aachen University for support with the construction of the reactor and the gas lines, N. Lothmann, B. Hermanns, and T. Storp for support with XRD measurements. Additionally, support and resources for the XPS experiments by L. Patterer and Prof. M. Schneider from the Institute for Materials Chemistry, RWTH Aachen University, is gratefully acknowledged. We thank the Helmholtz-Zentrum Berlin für Materialien und Energie for the allocation of synchrotron radiation beamtime and S. Cramm for experimental support of the XAS experiments.

AUTHOR INFORMATION

Corresponding Author

Daniel Röhrens - Institute of Inorganic Chemistry, RWTH Aachen University, Landoltweg 1a, 52074 Aachen, Germany; https://orcid.org/0000-0002-9690-2468;

Email: daniel.roehrens@ac.rwth-aachen.de

David N. Mueller - Peter Grünberg Institut, Forschungszentrum Jülich GmbH, 52428 Jülich, Germany; https://orcid.org/0000-0002-1062-6985; Email: dav.mueller@fz-juelich.de

Authors

Daniel Röhrens - Institute of Inorganic Chemistry, RWTH Aachen University, Landoltweg 1a, 52074 Aachen, Germany; https://orcid.org/0000-0002-9690-2468;

Ahed Abouserie - Institute of Inorganic Chemistry, RWTH Aachen University, Landoltweg 1a, 52074 Aachen, Germany; https://orcid.org/0000-0001-5435-5665

Gianluca Dalfollo - Institute of Inorganic Chemistry, RWTH Aachen University, Landoltweg 1a, 52074 Aachen, Germany

Jannis Kahlert - Institute of Inorganic Chemistry, RWTH Aachen University, Landoltweg 1a, 52074 Aachen, Germany

Bangfen Wang - Institute of Inorganic Chemistry, RWTH Aachen University, Landoltweg 1a, 52074 Aachen, Germany

Ariel Augusto Schönberger - Chair of Thermodynamics of Mobile Energy Conversion Systems, RWTH Aachen University, Forckenbeckstraße 4, 52074 Aachen, Germany; https://orcid.org/0000-0002-0490-1178

Stefan Pischinger - Chair of Thermodynamics of Mobile Energy Conversion Systems, RWTH Aachen University, Forckenbeckstraße 4, 52074 Aachen, Germany; https://orcid.org/0000-0002-0222-3457

Peirong Chen - Guangdong Provincial Key Laboratory of Atmospheric Environment and Pollution Control, National Engineering Laboratory for VOCs Pollution Control Technology and Equipment, School of Environment and Energy, South China University of Technology, Guangzhou 510006, China; https://orcid.org/0000-0003-1014-8044

David N. Mueller - Peter Grünberg Institut, Forschungszentrum Jülich GmbH, 52428 Jülich, Germany; https://orcid.org/0000-0002-1062-6985

Ulrich Simon - Institute of Inorganic Chemistry, RWTH Aachen University, Landoltweg 1a, 52074 Aachen, Germany; https://orcid.org/0000-0002-6118-0573

Author Contributions

The manuscript was written through contributions of all authors. All authors have given approval to the final version of the manuscript.

Notes

The authors declare no competing financial interest.

REFERENCES

- (1) Burkardt, P.; Ottenwälder, T.; König, A.; Viell, J.; Mitsos, A.; Wouters, C.; Marquardt, W.; Pischinger, S.; Dahmen, M. Toward Co-Optimization of Renewable Fuel Blend Production and Combustion in ultra-high Efficiency SI Engines. *International Journal of Engine Research* **2021**, 56 (1). DOI: 10.1177/14680874211040995.
- (2) Leitner, W.; Klankermayer, J.; Pischinger, S.; Pitsch, H.; Kohse-Höinghaus, K. Advanced Biofuels and Beyond: Chemistry Solutions for Propulsion and Production. *Angewandte Chemie International Edition* **2017**, *56* (20), 5412-5452. DOI: https://doi.org/10.1002/anie.201607257.
- (3) Noh, H. K.; No, S.-Y. Effect of Bioethanol on Combustion and Emissions in advanced CI Engines: HCCI, PPC and GCI Mode A Review. *Applied Energy* **2017**, *208*, 782-802. DOI: https://doi.org/10.1016/j.apenergy.2017.09.071.
- (4) Royer, S.; Duprez, D.; Can, F.; Courtois, X.; Batiot-Dupeyrat, C.; Laassiri, S.; Alamdari, H. Perovskites as Substitutes of Noble Metals for Heterogeneous Catalysis: Dream or Reality. *Chemical Reviews* **2014**, *114* (20), 10292-10368. DOI: 10.1021/cr500032a.
- (5) Jabłońska, M.; Palkovits, R. Perovskite-based Catalysts for the Control of Nitrogen Oxide Emissions from Diesel Engines. *Catalysis Science & Technology* **2019**, *9* (9), 2057-2077, 10.1039/C8CY02458H. DOI: 10.1039/C8CY02458H.

- (6) Liu, W.; Flytzani-Stephanopoulos, M. Transition Metal-promoted Oxidation Catalysis by Fluorite Oxides: A study of CO Oxidation over Cu.CeO2. *The Chemical Engineering Journal and the Biochemical Engineering Journal* **1996**, *64* (2), 283-294. DOI: https://doi.org/10.1016/S0923-0467(96)03135-1.
- (7) Libby, W. F. Promising Catalyst for Auto Exhaust. *Science* **1971**, *171* (3970), 499-500. DOI: doi:10.1126/science.171.3970.499.
- (8) Voorhoeve, R. J. H.; Remeika, J. P.; Freeland, P. E.; Matthias, B. T. Rare-Earth Oxides of Manganese and Cobalt Rival Platinum for the Treatment of Carbon Monoxide in Auto Exhaust. *Science* **1972**, *177* (4046), 353-354. DOI: doi:10.1126/science.177.4046.353.
- (9) Nitadori, T.; Misono, M. Catalytic properties of La(1–x)AxFeO3(A = Sr,Ce) and La(1–x)CexCoO3. *Journal of Catalysis* **1985**, *93* (2), 459-466. DOI: https://doi.org/10.1016/0021-9517(85)90193-9.
- (10) Keav, S.; Matam, S. K.; Ferri, D.; Weidenkaff, A. Structured Perovskite-Based Catalysts and Their Application as Three-Way Catalytic Converters—A Review. *Catalysts* **2014**, *4* (3), 226-255.
- (11) Wu, X.; Fischer, M.; Nolte, A.; Lenßen, P.; Wang, B.; Ohlerth, T.; Wöll, D.; Heufer, K. A.; Pischinger, S.; Simon, U. Perovskite Catalyst for In-Cylinder Coating to Reduce Raw Pollutant Emissions of Internal Combustion Engines. *ACS Omega* **2022**, *7* (6), 5340-5349. DOI: 10.1021/acsomega.1c06530.

- (12) Hong, W. T.; Welsch, R. E.; Shao-Horn, Y. Descriptors of Oxygen-Evolution Activity for Oxides: A Statistical Evaluation. *The Journal of Physical Chemistry C* **2016**, *120* (1), 78-86. DOI: 10.1021/acs.jpcc.5b10071.
- (13) Mefford, J. T.; Rong, X.; Abakumov, A. M.; Hardin, W. G.; Dai, S.; Kolpak, A. M.; Johnston, K. P.; Stevenson, K. J. Water Electrolysis on La1–xSrxCoO3–δ Perovskite Electrocatalysts. *Nature Communications* **2016**, *7* (1), 11053. DOI: 10.1038/ncomms11053.
- (14) Taihei, N.; Tatsumi, I.; Makoto, M. Catalytic Properties of Perovskite-Type Mixed Oxides (ABO3) Consisting of Rare Earth and 3d Transition Metals. The Roles of the A- and B-Site Ions. *Bulletin of the Chemical Society of Japan* **1988**, *61* (3), 621-626. DOI: 10.1246/bcsj.61.621.
- (15) Einaga, H.; Nasu, Y.; Oda, M.; Saito, H. Catalytic Performances of Perovskite Oxides for CO Oxidation under Microwave Irradiation. *Chemical Engineering Journal* **2016**, *283*, 97-104. DOI: https://doi.org/10.1016/j.cej.2015.07.051.
- (16) Li, H.; Shen, M.; Wang, J.; Wang, H.; Wang, J. Effect of Support on CO Oxidation Performance over the Pd/CeO2 and Pd/CeO2–ZrO2 Catalyst. *Industrial & Engineering Chemistry Research* **2020**, *59* (4), 1477-1486. DOI: 10.1021/acs.iecr.9b05351.
- (17) Yang, L.; Lin, S.; Yang, X.; Fang, W.; Zhou, R. Promoting Effect of Alkaline Earth Metal Doping on Catalytic Activity of HC and NOx Conversion over Pd-only Three-way Catalyst. *Journal of Hazardous Materials* **2014**, *279*, 226-235. DOI: https://doi.org/10.1016/j.jhazmat.2014.06.076.
- (18) Lang, W.; Laing, P.; Cheng, Y.; Hubbard, C.; Harold, M. P. Co-oxidation of CO and Propylene on Pd/CeO2-ZrO2 and Pd/Al2O3 Monolith Catalysts: A Light-off, Kinetics, and

- Mechanistic study. *Applied Catalysis B: Environmental* **2017**, *218*, 430-442. DOI: https://doi.org/10.1016/j.apcatb.2017.06.064.
- (19) Horikoshi, S.; Serpone, N. Role of Microwaves in Heterogeneous Catalytic Systems. *Catalysis Science & Technology* **2014**, *4* (5), 1197-1210, 10.1039/C3CY00753G. DOI: 10.1039/C3CY00753G.
- (20) Palma, V.; Barba, D.; Cortese, M.; Martino, M.; Renda, S.; Meloni, E. Microwaves and Heterogeneous Catalysis: A Review on Selected Catalytic Processes. *Catalysts* **2020**, *10* (2), 246.
- (21) Bao, C.; Serrano-Lotina, A.; Niu, M.; Portela, R.; Li, Y.; Lim, K. H.; Liu, P.; Wang, W.-j.; Bañares, M. A.; Wang, Q. Microwave-associated Chemistry in Environmental Catalysis for Air Pollution Remediation: A Review. *Chemical Engineering Journal* **2023**, *466*, 142902. DOI: https://doi.org/10.1016/j.cej.2023.142902.
- (22) Li, H.; Zhang, C.; Pang, C.; Li, X.; Gao, X. The Advances in the Special Microwave Effects of the Heterogeneous Catalytic Reactions. *Frontiers in Chemistry* **2020**, *8*, Review. DOI: 10.3389/fchem.2020.00355.
- (23) Röhrens, D.; Abouserie, A.; Wang, B.; Haselmann, G.; Simon, U. Microwave-Assisted CO Oxidation over Perovskites as a Model Reaction for Exhaust Aftertreatment A Critical Assessment of Opportunities and Challenges. *Catalysts* **2022**, *12* (7), 802.
- (24) Mishra, R. R.; Sharma, A. K. Microwave–material interaction phenomena: Heating Mechanisms, Challenges and Opportunities in Material Processing. *Composites Part A: Applied Science and Manufacturing* **2016**, *81*, 78-97. DOI: https://doi.org/10.1016/j.compositesa.2015.10.035.

- (25) Ano, T.; Tsubaki, S.; Liu, A.; Matsuhisa, M.; Fujii, S.; Motokura, K.; Chun, W.-J.; Wada, Y. Probing the Temperature of Supported Platinum Nanoparticles under Microwave Irradiation by in situ and operando XAFS. *Communications Chemistry* **2020**, *3* (1), 86. DOI: 10.1038/s42004-020-0333-y.
- (26) Beckers, J.; van der Zande, L. M.; Rothenberg, G. Clean Diesel Power via Microwave Susceptible Oxidation Catalysts. *ChemPhysChem* **2006**, *7* (3), 747-755. DOI: https://doi.org/10.1002/cphc.200500420.
- (27) Krech, T.; Möser, C.; Emmerich, R.; Scholz, P.; Ondruschka, B.; Cihlar, J. Catalytic and Heating Behavior of Nanoscaled Perovskites under Microwave Radiation. *Chemical Engineering & Technology* **2008**, *31* (7), 1000-1006. DOI: https://doi.org/10.1002/ceat.200700502.
- (28) Nishioka, M.; Miyakawa, M.; Daino, Y.; Kataoka, H.; Koda, H.; Sato, K.; Suzuki, T. M. Single-Mode Microwave Reactor Used for Continuous Flow Reactions under Elevated Pressure. *Industrial & Engineering Chemistry Research* **2013**, *52* (12), 4683-4687. DOI: 10.1021/ie400199r.
- (29) Will, H.; Scholz, P.; Ondruschka, B. Heterogeneous Gas-Phase Catalysis Under Microwave Irradiation—a New Multi-Mode Microwave Applicator. *Topics in Catalysis* **2004**, *29* (3), 175-182. DOI: 10.1023/B:TOCA.0000029800.57024.7d.
- (30) Stankiewicz, A.; Sarabi, F. E.; Baubaid, A.; Yan, P.; Nigar, H. Perspectives of Microwaves-Enhanced Heterogeneous Catalytic Gas-Phase Processes in Flow Systems. *The Chemical Record* **2019**, *19* (1), 40-50. DOI: https://doi.org/10.1002/tcr.201800070.

- (31) Serra, J. M.; Borrás-Morell, J. F.; García-Baños, B.; Balaguer, M.; Plaza-González, P.; Santos-Blasco, J.; Catalán-Martínez, D.; Navarrete, L.; Catalá-Civera, J. M. Hydrogen Production via Microwave-induced Water Splitting at low Temperature. *Nature Energy* **2020**, *5* (11), 910-919. DOI: 10.1038/s41560-020-00720-6.
- (32) Serra, J. M.; Balaguer, M.; Santos-Blasco, J.; Borras, J.; Garcia-Baños, B.; Plaza-González, P. J.; Catalán-Martínez, D.; Penaranda-Foix, F. L.; Dominguez, A.; Navarrete, L.; et al. Modulating Redox Properties of Solid-State Ion-Conducting Materials using Microwave Irradiation. *Materials Horizons* **2023**, 10, 5796-5894. DOI: 10.1039/D3MH01339A.
- (33) Andrushkevich, T. V.; Ovchinnikova, E. V. The Role of Water in Selective Heterogeneous Catalytic Oxidation of Hydrocarbons. *Molecular Catalysis* **2020**, *484*, 110734. DOI: https://doi.org/10.1016/j.mcat.2019.110734.
- (34) Kishimoto, F.; Yoshioka, T.; Ishibashi, R.; Yamada, H.; Muraoka, K.; Taniguchi, H.; Wakihara, T.; Takanabe, K. Direct microwave energy input on a single cation for outstanding selective catalysis. *Science Advances* **2023**, *9* (33), 1744. DOI: doi:10.1126/sciadv.adi1744.
- (35) Dreyer, M.; Cruz, D.; Hagemann, U.; Zeller, P.; Heidelmann, M.; Salamon, S.; Landers, J.; Rabe, A.; Ortega, K. F.; Najafishirtari, S.; et al. The Effect of Water on the 2-Propanol Oxidation Activity of Co-Substituted LaFe1–xCoxO3 Perovskites. *Chemistry A European Journal* **2021**, 27 (68), 17127-17144. DOI: https://doi.org/10.1002/chem.202102791.
- (36) Falk, T.; Budiyanto, E.; Dreyer, M.; Pflieger, C.; Waffel, D.; Büker, J.; Weidenthaler, C.; Ortega, K. F.; Behrens, M.; Tüysüz, H.; et al. Identification of Active Sites in the Catalytic Oxidation of 2-Propanol over Co1+xFe2-xO4 Spinel Oxides at Solid/Liquid and Solid/Gas

- Interfaces. *ChemCatChem* **2021**, *13* (12), 2942-2951. DOI: https://doi.org/10.1002/cctc.202100352.
- (37) Lamb, A. B.; Vail, W. E. The Effect Of Water And Of Carbon Dioxide On The Catalytic Oxidation Of Carbon Monoxide And Hydrogen By Oxygen. *Journal of the American Chemical Society* **1925**, *47* (1), 123-142. DOI: 10.1021/ja01678a018.
- (38) Mullen, G. M.; Evans, E. J.; Sabzevari, I.; Long, B. E.; Alhazmi, K.; Chandler, B. D.; Mullins, C. B. Water Influences the Activity and Selectivity of Ceria-Supported Gold Catalysts for Oxidative Dehydrogenation and Esterification of Ethanol. *ACS Catalysis* **2017**, *7* (2), 1216-1226. DOI: 10.1021/acscatal.6b02960.
- (39) Song, S.; Zhang, S.; Zhang, X.; Verma, P.; Wen, M. Advances in Catalytic Oxidation of Volatile Organic Compounds over Pd-Supported Catalysts: Recent Trends and Challenges. *Frontiers in Materials* **2020**, *7*, Review. DOI: 10.3389/fmats.2020.595667.
- (40) Wang, Y.; Zhu, X.; Crocker, M.; Chen, B.; Shi, C. A Comparative Study of the Catalytic Oxidation of HCHO and CO over Mn0.75Co2.25O4 Catalyst: The Effect of Moisture. *Applied Catalysis B: Environmental* **2014**, *160-161*, 542-551. DOI: https://doi.org/10.1016/j.apcatb.2014.06.011.
- (41) Caporali, R.; Chansai, S.; Burch, R.; Delgado, J. J.; Goguet, A.; Hardacre, C.; Mantarosie, L.; Thompsett, D. Critical Role of Water in the Direct Oxidation of CO and Hydrocarbons in Diesel Exhaust After Treatment Catalysis. *Applied Catalysis B: Environmental* **2014**, *147*, 764-769. DOI: https://doi.org/10.1016/j.apcatb.2013.10.004.

- (42) Yan, X.; Huang, Q.; Li, B.; Xu, X.; Chen, Y.; Zhu, S.; Shen, S. Catalytic Performance of LaCo0.5M0.5O3 (M=Mn, Cr, Fe, Ni, Cu) Perovskite-type Oxides and LaCo0.5Mn0.5O3 Supported on Cordierite for CO Oxidation. *Journal of Industrial and Engineering Chemistry* **2013**, *19* (2), 561-565. DOI: https://doi.org/10.1016/j.jiec.2012.09.026.
- (43) Jiang, B.-S.; Chang, R.; Lin, Y.-C. Partial Oxidation of Ethanol to Acetaldehyde over LaMnO3-Based Perovskites: A Kinetic Study. *Industrial & Engineering Chemistry Research* **2013**, *52* (1), 37-42. DOI: 10.1021/ie300348u.
- (44) Wu, Y.; Cordier, C.; Berrier, E.; Nuns, N.; Dujardin, C.; Granger, P. Surface Reconstructions of LaCo1–xFexO3 at High Temperature during N2O Decomposition in Realistic Exhaust Gas Composition: Impact on the Catalytic Properties. *Applied Catalysis B: Environmental* **2013**, *140-141*, 151-163. DOI: https://doi.org/10.1016/j.apcatb.2013.04.002.
- (45) Shirley, D. A. High-Resolution X-Ray Photoemission Spectrum of the Valence Bands of Gold. *Physical Review B* **1972**, *5* (12), 4709-4714. DOI: 10.1103/PhysRevB.5.4709.
- (46) Tatsuo, O.; Akiko, W. Simple Suppressing Method of Thermal Runaway in Microwave Heating of Zeolite and its Application. *PhysChemComm* **2001**, *4* (3), 18-20, 10.1039/B009067K. DOI: 10.1039/B009067K.
- (47) Wu, X.; Thomas, J. R., Jr.; Davis, W. A. Control of Thermal Runaway in Microwave Resonant Cavities. *Journal of Applied Physics* **2002**, *92* (6), 3374-3380. DOI: 10.1063/1.1501744
- (48) Yang, J.; Hu, S.; Fang, Y.; Hoang, S.; Li, L.; Yang, W.; Liang, Z.; Wu, J.; Hu, J.; Xiao, W.; et al. Oxygen Vacancy Promoted O2 Activation over Perovskite Oxide for Low-Temperature CO Oxidation. *ACS Catalysis* **2019**, *9* (11), 9751-9763. DOI: 10.1021/acscatal.9b02408.

- (49) Jain, R.; Gnanakumar, E. S.; Gopinath, C. S. Mechanistic Aspects of Wet and Dry CO Oxidation on Co3O4 Nanorod Surfaces: A NAP-UPS Study. *ACS Omega* **2017**, *2* (3), 828-834. DOI: 10.1021/acsomega.6b00471.
- (50) Zhao, S.; Chen, F.; Duan, S.; Shao, B.; Li, T.; Tang, H.; Lin, Q.; Zhang, J.; Li, L.; Huang, J.; et al. Remarkable Active-Site Dependent H2O Promoting Effect in CO Oxidation. *Nature Communications* **2019**, *10* (1), 3824. DOI: 10.1038/s41467-019-11871-w.
- (51) Mutoro, E.; Crumlin, E. J.; Pöpke, H.; Luerssen, B.; Amati, M.; Abyaneh, M. K.; Biegalski, M. D.; Christen, H. M.; Gregoratti, L.; Janek, J.; et al. Reversible Compositional Control of Oxide Surfaces by Electrochemical Potentials. *The Journal of Physical Chemistry Letters* **2012**, *3* (1), 40-44. DOI: 10.1021/jz201523y.
- (52) Feng, Z.; Crumlin, E. J.; Hong, W. T.; Lee, D.; Mutoro, E.; Biegalski, M. D.; Zhou, H.; Bluhm, H.; Christen, H. M.; Shao-Horn, Y. In Situ Studies of the Temperature-Dependent Surface Structure and Chemistry of Single-Crystalline (001)-Oriented La0.8Sr0.2CoO3-δ Perovskite Thin Films. *The Journal of Physical Chemistry Letters* **2013**, *4* (9), 1512-1518. DOI: 10.1021/jz400250t.
- (53) Chainani, A.; Mathew, M.; Sarma, D. D. Electron-Spectroscopy Study of the Semiconductor-Metal Transition in La1-xSrxCoO3. *Physical Review B* **1992**, *46* (16), 9976-9983. DOI: 10.1103/PhysRevB.46.9976.
- (54) Geatches, D. L.; Metz, S.; Mueller, D. N.; Wilcox, J. An ab initio Characterization of the Electronic Structure of LaCoxFe1–xO3 for x ≤ 0.5 (Phys. Status Solidi B 9/2016). *physica status solidi (b)* **2016**, *253* (9), 1665-1665. DOI: https://doi.org/10.1002/pssb.201670557.

- (55) Abbate, M.; Fuggle, J. C.; Fujimori, A.; Tjeng, L. H.; Chen, C. T.; Potze, R.; Sawatzky, G. A.; Eisaki, H.; Uchida, S. Electronic Structure and Spin-State Transition of LaCoO3. *Physical Review B* **1993**, *47* (24), 16124-16130. DOI: 10.1103/PhysRevB.47.16124.
- (56) Lam, D. J.; Veal, B. W.; Ellis, D. E. Electronic Structure of Lanthanum Perovskites with 3d Transition Elements. *Physical Review B* **1980**, *22* (12), 5730-5739. DOI: 10.1103/PhysRevB.22.5730.
- (57) Biesinger, M. C.; Payne, B. P.; Grosvenor, A. P.; Lau, L. W. M.; Gerson, A. R.; Smart, R. S. C. Resolving Surface Chemical States in XPS Analysis of First Row Transition Metals, Oxides and Hydroxides: Cr, Mn, Fe, Co and Ni. *Applied Surface Science* **2011**, *257* (7), 2717-2730. DOI: https://doi.org/10.1016/j.apsusc.2010.10.051.
- (58) Medling, S.; Lee, Y.; Zheng, H.; Mitchell, J. F.; Freeland, J. W.; Harmon, B. N.; Bridges, F. Evolution of Magnetic Oxygen States in Sr-Doped LaCoO3. *Physical Review Letters* **2012**, *109* (15), 157204. DOI: 10.1103/PhysRevLett.109.157204.
- (59) Mueller, D. N.; Machala, M. L.; Bluhm, H.; Chueh, W. C. Redox Activity of Surface Oxygen Anions in Oxygen-Deficient Perovskite Oxides during Electrochemical Reactions. *Nature Communications* **2015**, *6* (1), 6097. DOI: 10.1038/ncomms7097.
- (60) Tong, Y.; Guo, Y.; Chen, P.; Liu, H.; Zhang, M.; Zhang, L.; Yan, W.; Chu, W.; Wu, C.; Xie, Y. Spin-State Regulation of Perovskite Cobaltite to Realize Enhanced Oxygen Evolution Activity. *Chem* **2017**, *3* (5), 812-821. DOI: https://doi.org/10.1016/j.chempr.2017.09.003.
- (61) Abbate, M.; de Groot, F. M. F.; Fuggle, J. C.; Fujimori, A.; Strebel, O.; Lopez, F.; Domke, M.; Kaindl, G.; Sawatzky, G. A.; Takano, M.; et al. Controlled-Valence Properties of La1-x Sr x

- FeO3 and La1-x Sr x MnO3 Studied by Soft-X-Ray Absorption Spectroscopy. *Physical Review B* **1992**, *46* (8), 4511-4519. DOI: 10.1103/PhysRevB.46.4511.
- (62) van der Heide, P. A. W. Systematic X-Ray Photoelectron Spectroscopic Study of La1–xSrx-based Perovskite-Type Oxides. *Surface and Interface Analysis* **2002**, *33* (5), 414-425. DOI: https://doi.org/10.1002/sia.1227.
- (63) Hashimoto, S.-i.; Fukuda, Y.; Kuhn, M.; Sato, K.; Yashiro, K.; Mizusaki, J. Oxygen Nonstoichiometry and Thermo-Chemical Stability of La0.6Sr0.4Co1-yFeyO3-δ (y=0.2, 0.4, 0.6, 0.8). *Solid State Ionics* **2010**, *181* (37), 1713-1719. DOI: https://doi.org/10.1016/j.ssi.2010.09.024.
- (64) Kuhn, M.; Hashimoto, S.; Sato, K.; Yashiro, K.; Mizusaki, J. Oxygen Nonstoichiometry and Thermo-Chemical Stability of La0.6Sr0.4CoO3-δ. *Journal of Solid State Chemistry* **2013**, 197, 38-45. DOI: https://doi.org/10.1016/j.jssc.2012.08.001.
- (65) Wang, X.; Huang, K.; Yuan, L.; Xi, S.; Yan, W.; Geng, Z.; Cong, Y.; Sun, Y.; Tan, H.; Wu, X.; et al. Activation of Surface Oxygen Sites in a Cobalt-Based Perovskite Model Catalyst for CO Oxidation. *The Journal of Physical Chemistry Letters* **2018**, *9* (15), 4146-4154. DOI: 10.1021/acs.jpclett.8b01623.
- (66) Mizusaki, J.; Mima, Y.; Yamauchi, S.; Fueki, K.; Tagawa, H. Nonstoichiometry of the Perovskite-Type Oxides La1–xSrxCoO3–δ. *Journal of Solid State Chemistry* **1989**, 80 (1), 102-111. DOI: https://doi.org/10.1016/0022-4596(89)90036-4.

TOC graphic:

